A brief review on strain engineering of ferroelectric $K_xNa_{1-x}NbO_3$ epitaxial thin films: insights from phase-field simulations

Bo Wang[1,*], Mengjun Zhou[2], Tiannan Yang[3], Long-Qing Chen[4,*]

[1] *Materials Science Division, Lawrence Livermore National Laboratory, California 94550, USA*

[2] *State Key Laboratory of Advanced Technology for Materials Synthesis and Processing, Center of Smart Materials and Devices, School of Materials Science and Engineering, Wuhan University of Technology, No.122 Luoshi Road, Wuhan 430070, P. R. China*

[3] *Interdisciplinary Research Center, School of Mechanical Engineering, Shanghai Jiao Tong University, Shanghai 200240, China*

[4] *Materials Research Institute and Department of Materials Science and Engineering, The Pennsylvania State University, University Park, Pennsylvania 16802, USA*

[*]corresponding author: wang111@llnl.gov (B.W.), lqc3@psu.edu (L.Q.C.)

Keywords: domains and domain walls, ferroelectric phases, material properties, phase-field model

Abstract (150 words)

Strains play a pivotal role in determining the phase equilibrium, domain configuration, and functional properties of low-dimensional ferroelectrics. There is growing interest in the strain engineering of ferroelectric $K_xNa_{1-x}NbO_3$ (KNN) epitaxial thin films, which exhibit excellent physical properties and promise as eco-friendly alternatives to lead-based ferroelectrics for microdevice applications. Advances have been made in understanding the phase equilibria and transitions, domains and domain walls, and their relations to the physical properties of KNN epitaxial thin films using a combination of experiments and theoretical modeling, particularly phase-field simulations. Here, we review recent progress in these aspects and showcase the phase-field method for establishing strain phase diagrams, elucidating the domain and domain wall structures at equilibrium, and predicting the structure–property relationships in ferroelectric KNN thin films. We also discuss challenges and opportunities to further advance our understanding of KNN thin films and potentially unlock new functionalities by leveraging phase-field simulations.

1 Introduction

Ferroelectric thin films have garnered significant research interest over the past decades due to their promising technological applications and fundamental scientific importance[1,2]. These materials exhibit a unique set of physical properties, such as high dielectric permittivity, large piezoelectric activity, nonlinear optical susceptibilities, and switchable spontaneous polarization, making them suitable for various functional devices, including high energy-density capacitors[3], microelectromechanical systems[4], integrated photonics[5], and non-volatile memories[6]. Furthermore, the reduced dimensionality of ferroelectric thin films and their tunable mechanical and electrical boundary conditions allow for investigations of novel ferroelectric phases and domain structures with unique physical behaviors distinct from those of their bulk counterparts[2].

Strain can be employed to tune the phase stability and thus the functional properties of ferroelectric thin films[7]. To fully exploit the potential of ferroelectric thin films, it is essential to understand the correlations among misfit strains, ferroelectric phases and domains, and their corresponding macroscopic properties. Significant progress has been made in the strain engineering of classical ferroelectric perovskite oxides such as $PbTiO_3$ (PTO)[8], $BaTiO_3$ (BTO)[9], and $BiFeO_3$ (BFO)[10]. At room temperature, these bulk crystals exhibit either tetragonal or rhombohedral ferroelectric phases. New ferroelectric phases can be stabilized by imposing misfit strains through epitaxial growth, e.g., monoclinic phases in BFO epitaxial thin films[10]. While epitaxial strains generally suppress the intrinsic piezoelectric coefficient, the multiphase/multidomain states stabilized by epitaxial strains may enhance piezoelectric responses[11]. However, it is still poorly understood how misfit strains affect the stability of the orthorhombic ferroelectric phase, another common polymorphic phase of perovskite oxides, and the corresponding physical properties.

The solid solution between $KNbO_3$ (KNO) and $NaNbO_3$ (NNO), i.e., $K_xNa_{1-x}NbO_3$ (KNN), is an ideal model system for such studies. In bulk KNO, there are structural phases isostructural to those of BTO, transitioning from cubic (*Pm*3*m*) to tetragonal (*P*4*mm*), orthorhombic (*Amm*2), and rhombohedral (*R*3*c*) phases as the temperature decreases from 800K to 100 K [12,13](Figure 1a). The same transition sequence is maintained in KNN solid solutions with up to 50% NNO (i.e., $K_{0.5}Na_{0.5}NbO_3$) [14,15](Figure 1b). The other endmember, NNO, exhibits a more complex series of phase transitions due to the involvement of the oxygen octahedral tilts [16]. As it cools from the high-temperature cubic phase, bulk NNO undergoes six non-ferroelectric phases until reaching a rhombohedral ferroelectric phase below 173K. At room temperature, NNO exhibits an antiferroelectric orthorhombic phase (*Pbcm*) that can transition to a metastable orthorhombic ferroelectric phase ($Pmc2_1$ or $P2_1ma$) under a moderate electric field[17](Figure 1c). Consequently, the temperature-composition phase diagram of KNN is rather complex [18,19] (Figure 1d), offering a rich landscape to explore the interplay among the ferroelectric, antiferroelectric, and antiferrodistortive orderings[20]. KNN-based crystals and ceramics are emerging as promising lead-free alternatives to lead-containing ferroelectric materials like $Pb(Zr_{1-x}Ti_x)O_3$(PZT), attracting attention due to increasing concerns about ecological sustainability[21,22]. In fact, high dielectric tunability[23], giant piezoelectric strains [24,25], highly sensitive and potential selective surface acoustic wave detection [26], and exceptional high elasto-optical coefficients [27] have been reported in strain-engineered KNN thin films, making the study of their structures and properties of both scientific interest and technological relevance.

Several comprehensive review articles have documented progress in developing KNN-based ceramics [22], single crystals [28], and thin films [29–31] from experimental perspectives. However, recent advances in the use of theoretical tools[32–35], particularly phase-field modeling[36], to the KNN

ferroelectric thin films have provided profound insights into the phase equilibria and transitions, domain and domain wall structures, and their correlation to macroscopic material properties[37–39]. This brief review presents the state-of-the-art by summarizing the experimental and theoretical understandings of ferroelectric phase transitions, domain and superdomain structures at equilibrium, and the corresponding functional properties in KNN epitaxial thin films. In the following sections, we first summarize the experimental findings related to the phase symmetries and domain morphologies of KNN epitaxial thin films. We then outline a general framework for establishing phase-field models for ferroelectric materials. Subsequently, we review the progress made in the theoretical modeling of KNN thin films, including the development of thermodynamic models of KNN, construction of strain phase diagrams, and determination of the equilibrium structures of domains, domain walls, and superdomain structures. Finally, we discuss the challenges and opportunities to exploit the phase-field approach to advance our understanding of KNN-based ferroelectric materials and their applications.

2 Experimental studies of ferroelectric KNN epitaxial thin films

In this section, we summarize the state-of-the-art experimental results on the characterization of ferroelectric phases, equilibrium domain morphology, and domain wall configurations in KNN thin films with various compositions grown on different substrate materials. We discuss a unified picture of the strain effect on the phase equilibria of K-rich KNN and NNO epitaxial thin films and highlight three typical domain patterns of ferroelectric KNN thin films.

Before describing the technical details, we provide two preliminary notes. First, significant efforts have been made to epitaxially grow KNN films using pulsed laser deposition[40–43], hydrothermal methods[44], RF magnetron sputtering[45–47], chemical solution deposition[48], metal-

organic vapor-phase epitaxy[30], sol-gel methods[49], among others[29]. However, we focus only on studies reporting ferroelectric phases that differ from bulk states and on characterizing domain structures influenced by misfit strains imposed by the substrate materials. Second, various notations have been used to represent ferroelectric phases in perovskite oxide thin films in the literature, which often leads to confusion. Here, we adopt a notation based on the crystal system of *the conventional unit cell* (e.g., monoclinic, orthorhombic) and the spontaneous polarization direction within *the pseudocubic unit cell* of the perovskite structure (e.g., a_1, a_2, c). Examples include the orthorhombic c-phase with $\boldsymbol{P}$ = (0, 0, P_3), monoclinic a_1c-phase with $\boldsymbol{P}$ = (P_1, 0, P_3) and a_2c-phase with $\boldsymbol{P}$ = (0, P_2, P_3), and monoclinic a_1a_2-phase with $\boldsymbol{P}$ = (P_1, P_2, 0). We refer to both a_1c- and a_2c-phases as M_C-phase. The M_A- and M_B-phases with $\boldsymbol{P}$ = (P_1, P_2, P_3) are distinguished by the relative amplitude of the polarization components, i.e., $P_1 = P_2 < P_3$ for M_A and $P_1 = P_2 < P_3$ for M_B. A detailed discussion on the notation of ferroelectric phases is given by Janolin[50].

2.1 Ferroelectric phases

Table 1 summarizes several new ferroelectric phases absent in bulk states reported in epitaxial KNN thin films, including the monoclinic M_A-, M_B-, a_1a_2-, and M_C-phases, as well as orthorhombic c, a_1, and a_2 phases. These phases develop under various film compositions, growth conditions, and substrate types and can be broadly categorized into four types based on misfit strain states (Table 2).

For K-rich KNN thin films (x > 0.5), highly biaxial compressive strains induce the monodomain orthorhombic c-phase, which is observed in fully strained $Ka_{0.7}Na_{0.3}NbO_3$ films on the $DyScO_3$ (DSO) substrate[51,52]. Moderate biaxial compressive misfit strains provided by rare-earth scandates like $SmScO_3$ (SSO), $GdScO_3$ (GSO), and $TbScO_3$ (TSO), favor the monoclinic

M_C-phase[51,53]. Upon heating, the M_C-phase transforms into the orthorhombic *c*-phase[51] or monoclinic M_A-phase [49,54], depending on the film composition and substrate materials. When both tensile and compressive strains are applied orthogonally in-plane, the a_1a_2/M_C-phase is formed, as observed in $Ka_{0.9}Na_{0.1}NbO_3$ films on $NdScO_3$ substrates[55,56]. Subsequent heating of the a_1a_2/M_C-phase results in the orthorhombic a_1/a_2-phase with exclusively in-plane polarization[57].

For NNO, the lattice constants of its pseudocubic unit cell are smaller than those of $KNbO_3$ by nearly 0.1 Å [30]. Consequently, the lattice mismatch between NNO films and $ReScO_3$ (Re = Dy, Gd, Tb) substrates induces biaxial tensile strains, resulting in the monoclinic a_1a_2-phase with in-plane polarization[58,59]. Upon partial relaxation of such tensile strains, as observed in thicker films, the monoclinic a_1a_2-phase transitions into other monoclinic M_A- or M_B-phases with out-of-plane polarization[60]. Highly compressively strained NNO films on $NdGaO_3$ substrates exhibit an orthorhombic *c*-phase with only out-of-plane polarization[59,61]. Despite the distinct origins of ferroelectricity in bulk phases, similarities in strain-induced ferroelectric phases and phase transitions between KNN and NNO epitaxial thin films have been noted[62].

2.2 Ferroelectric domains and superdomains

The equilibrium domain structures of these ferroelectric phases in as-grown KNN and NNO films can be categorized into three types based on their two-dimensional morphology, which can be viewed from an out-of-plane perspective: monodomains, stripe-like domains, and herringbone-like domains.

In monodomains, uniform out-of-plane polarization with minimal in-plane variations has been reported in the orthorhombic *c*-phase of NNO thin films[58] and KNN thin films[51], as well as in other ultrathin films below the critical thickness for domain formation [52].

Stripe-like domains exhibit highly regular laminar patterns in both monoclinic and orthorhombic ferroelectric phases at various temperatures[30,53,57,62]. The patterns can be classified into one-dimensional and two-dimensional structures. The one-dimensional stripe-like patterns parallel to $[010]_{pc}$ emerge in a_1a_2-, M_A-, and M_B-phases of NNO[58,60]. The two-dimensional stripe-like domain patterns parallel to $[010]_{pc}$ and $[100]_{pc}$ have been found in M_A-phase of NNO on GSO substrates[58], while another two-dimensional pattern parallel to $[110]_{pc}$ and $[1\text{-}10]_{pc}$ is shown in the monoclinic M_C-phase of KNN films[49,49,53,63] and the orthorhombic a_1/a_2-phases of KNN [57] and NNO films[62]. Notably, the stripe-like domains of the M_C-phase show superdomain structures consisting of four energy-equivalent bundles of a_1c and a_2c domains[52,53].

Herringbone-like domain patterns are reported exclusively in the a_1a_2/M_C-phase of KNN [55,56,64]. They differ from the stripe-like domains in three ways. First, domain walls in the herringbone patterns do not follow any low-index directions but vary with film compositions and thickness[64]. Second, the herringbone pattern is hierarchical, where polydomains of a_1a_2- and M_C-phases self-assemble into superdomain structures with regular, well-defined boundaries[55,56]. In contrast, the superdomain boundary of the stripe-like domain patterns are irregular[52]. Third, the lattice constant differences between variants of the a_1a_2- and M_C-phases under anisotropic misfit strains mean that the interfaces between these domains are heterophase boundaries rather than conventional twin domain walls. The mechanical compatibility condition may not hold for the heterophase boundary[65,66]. Besides, the herringbone-like domains can transform into stripe-like domains of the high-temperature orthorhombic a_1/a_2-phase upon heating[57,67].

Two-dimensional piezoresponse force microscopy (PFM) images of these domain structures in KNN epitaxial thin films, along with their corresponding three-dimensional models

obtained through phase-field simulations, are highlighted in Figure 2a – c for the M_C-phase[53], a_1a_2/M_C-phase at room temperature[56], and a_1a_2/M_C-phase at elevated temperatures[57], respectively.

2.3 Ferroelectric domain walls

There have been few studies on the domain walls of KNN thin films. The domain walls of a_1a_2-phase of NNO resemble the 90° domain walls of the orthorhombic phase (*Amm*2) of bulk KNO and are determined to be parallel to $(100)_{pc}$ of the film[30]. Domain walls of M_C- and a_1a_2/M_C-phases resemble the 60° domain walls of the orthorhombic phase of bulk KNO modified by biaxial misfit strains. Mechanically compatible charge-neutral 60° domain walls of the orthorhombic phase are known as *S*-walls, the plane of which varies with local spontaneous strains [66]. Likewise, the domain walls of the monoclinic M_C-phase also show this attribute. Advanced diffraction techniques have been employed to determine the domain wall orientation of the a_1a_2/M_C-phase KNN and have revealed large variations of the domain wall plane with regard to film thickness and compositions[64]. The domain walls of the stripe-like domains of the M_C phase also differ from those of the $(011)_{pc}$ planes. In addition, charged domain walls have been identified in the M_C-phase of KNN films on DSO substrates deposited using the sol-gel method[63].

3 Phase-field methods to model ferroelectric materials

The phase-field method stands as a robust tool for investigating phase equilibria and transitions, microstructural features such as domains and domain walls, and the intricate microstructure-property relationship in ferroelectric materials and heterostructures[36]. Here, we provide an overview of the establishment of a phase-field model for ferroelectric materials.

A typical phase-field model for ferroelectrics comprises three essential components: order parameter(s), a thermodynamic model, and a kinetic model. For proper ferroelectrics, the

spontaneous polarization vector $\boldsymbol{P} = (P_1, P_2, P_3)$ often serves as the primary order parameter. It distinguishes between paraelectric and ferroelectric phases as well as various domain variants of ferroelectric phases. For example, the six domain variants of the tetragonal ferroelectric phase and cubic paraelectric phase can be represented by $(\pm P_1, 0, 0)$, $(0, \pm P_2, 0)$, $(0, 0, \pm P_3)$, and $(0, 0, 0)$, respectively. For improper/incipient ferroelectric materials, such as $SrTiO_3$ (STO), multiple coupled soft modes are required to drive phase transitions[68], necessitating additional sets of structural order parameters, e.g., a pseudovector order parameter $\boldsymbol{Q} = (Q_1, Q_2, Q_3)$, to represent the antiferrodistortive phase transition characterized by the oxygen octahedral tilt. To account for antiferroelectric transitions such as those in NNO, another order parameter for the antipolar ordering is required[69].

The thermodynamic free energy of an inhomogeneous ferroelectric can be formulated as a functional of the order parameters. The widely adopted Landau-Ginzburg-Devonshire (LGD) model employs a high-order polynomial of the order parameters to describe the bulk chemical contribution. The polynomial form adheres to the symmetry requirements derived from group-subgroup analyses[70]. The coefficients of the polynomial, which depend on the temperature and chemical composition, can be determined by fitting experimental data or by first-principles calculations. The short-range interactions of the order parameters are often approximated as a quadratic term of the spatial gradient of the order parameters, with material-dependent coefficients related to the domain wall energy. In addition, coupling effects between the order parameters and mechanical stress/strain can be incorporated as nonlinear effects, such as electrostriction, along with nonlocal effects, such as flexoelectricity[71].

Completing the phase-field model requires a kinetic description that governs the time evolution of the order parameters driven by the thermodynamic forces. Relaxational kinetics, such

as the time-dependent Ginzburg-Landau equation, are often assumed to efficiently attain equilibrium states. The mobility coefficient is typically assumed constant for simplicity, whereas generalized nonlinear kinetic models with mobility dependent on driving forces have also been proposed [72]. Alternative dynamical models, such as the Klein-Gordon type equation, are adopted to capture ultrafast polarization dynamics induced by strong external stimuli[73]. These dynamical models are supplemented by elastodynamic and electrodynamic equations[74,75], as the assumptions of mechanical and electrical equilibria do not hold.

Choosing appropriate boundary conditions for the time-dependent equations of the order parameters and associated equilibrium equations is crucial. Three-dimensional boundaries are standard for bulk ferroelectric crystals[76], while finite-size systems like epitaxial thin films require tailored boundary conditions at the film surface and film-substrate interface[77,78]. Additionally, numerical methods for space discretization and time integration significantly influence the efficiency of solving the phase-field equations. Detailed discussions on these methods can be found in specialized review articles and literature [36,79,80].

4 Theoretical studies on ferroelectric KNN epitaxial thin films

This section reviews recent theoretical advancements in understanding ferroelectric phases and transitions, domain and domain wall structures, and their influence on the macroscopic properties of KNN thin films. We focus on the development of thermodynamic models, construction of strain phase diagrams, and analyses of domain and superdomain structures using phase-field simulations.

4.1 Thermodynamic Model of KNN

A robust thermodynamic model forms the basis for phase-field modeling of ferroelectric materials like KNN. Liang *et al.* [81] developed an eighth-order LGD model for KNO, parameterized against experimental data for phase transition temperatures, dielectric permittivity, and piezoelectric coefficients[82]. This model was extended[32] to the K-rich side of KNN with $x = 0.5 \sim 1.0$. Using the thermodynamic model of KNN, various structural and thermodynamic properties can be calculated for KNN bulk crystals and thin films based on the monodomain assumption[83], including phase transition temperatures[33], spontaneous polarization and strains[32,84], electrocaloric coefficients[34,85], dielectric constants[85], and piezoelectric coefficients [33,35,84].

In contrast, a thermodynamic model for the Na-rich side of KNN remains elusive. The gap is likely due to the involvement of oxygen octahedral tilts for the NNO-rich side of the phase diagram (c.f. Figure 1d). Recent efforts by Hadaeghi *et al.* introduced a first-principles-based LGD-type model capable of describing ferroelectric-to-antiferroelectric phase transitions in Na-rich KNN using three coupled order parameters[86]. Nevertheless, the coupling coefficients of the order parameters to strains have not yet been determined, which limits its application to strained NNO thin films[87]. The coupling between the order parameters and the electric field is also critical in modeling the electric-field-induced antiferroelectric-to-ferroelectric transition in NNO[88].

4.2 Constructing strain phase diagrams

Strain phase diagrams are essential for predicting phase equilibria and selecting substrate materials for the desired properties of ferroelectric thin films. The temperature–strain phase diagram is adequate for describing the phase equilibria of thin films subjected to biaxial isotropic misfit strains, while for films subjected to biaxial anisotropic strains, the misfit strain–misfit strain diagram at room temperature is necessary. Various theoretical approaches have been employed,

including first-principles calculations[87,89], thermodynamic calculations[33,84,85,90,91], and phase-field simulations[37,38], to establish the strain phase diagrams of KNN.

The first-principles calculation-based method is predictive but generally limited to monodomain states. Dieguez *et al.* [89] calculated the *ab initio* phase diagram in terms of uniaxial stress and biaxial isotropic strain for KNO and NNO. It is predicted that the ferroelectric phase evolves from the *c*-phase to *r*-phase (corresponding to M_A or M_B-phase in our notation) and to *aa*-phase (corresponding to a_1a_2-phase in our notation) when the strain varies from compressive to tensile[89]. This trend has been verified in experiments for NNO thin films[59]. Very recently, other ground states of NNO under strains have been revealed by first-principles calculation[87]. In addition, atomistic simulation-based approaches have been utilized to construct the strain phase diagrams for other ferroelectric materials [92,93], while their employment for KNN thin films requires the development of well-parametrized effective Hamiltonian functionals or interatomic potentials for the system.

The thermodynamic calculations are usually based on *a priori* assumption on the domain states [83,94]. The monodomain strain phase diagrams of KNO [30,90] and KNN thin films [33,84,85,91] have been established using the thermodynamic models of bulk KNN[32,81], as shown in Figure 3a,b. The sequence of phase evolution by varying the strain from compressive to tensile is identical to the prediction of first-principles calculations at $T = 0$ K. The monodomain phase diagram agrees well with experiments predicting the orthorhombic *c*-phase of KNN[70] on DSO[51] and the M_A-phase KNN on STO at high temperature[49]. The strain phase diagrams can also be established using the thermodynamic theory for polydomains[95], yet its application to the KNN systems has not been reported.

The strain phase equilibrium theory[96,97] provides an alternative way to construct the strain phase diagram based on thermodynamics without assuming *a priori* multiphase/multidomain states. Using this method, Wang *et al.* obtained the polydomain strain phase diagrams of KNN subject to biaxially misfit strains[98], as shown in Figure 3d. Compared with the monodomain strain phase diagrams, the polydomain strain diagram reveals phase coexistence between the a_1c, a_2c, and a_1a_2-phases at low-strain states of KNN, which is consistent with the observation of M_C- and a_1a_2/M_C-phases[53,56]. The application of the strain phase equilibrium theory to the temperature-strain phase diagrams of KNN has also shown similaries to the diagram constructed using the phase-field approach[99].

Phase-field simulations complement the above approaches by providing detailed phase diagrams under varying strains and temperatures, offering additional insights into the domain structures. The obtained temperature–strain[37] and strain–strain phase diagrams[38] of KNN are shown in Figure 3e,f. Though computationally intensive, the diagrams obtained by phase-field simulations can accurately reproduce experimental observations and predict potential new domain structures not yet reported, thus providing a deeper understanding of phase transitions and microstructure evolution in KNN thin films.

4.3 Domains, domain walls, and superdomains at equilibrium

Strained KNN thin films can develop multiple ferroelastic domain variants to relieve the mechanical energy. Phase-field simulations are instrumental in modeling these complex systems and considering inhomogeneous stress distributions, electrical boundary conditions, and domain wall energies. Wang and Zhou *et al.* [37,38] utilized phase-field simulations to predict three-dimensional domain structures in KNN thin films under various strains and temperatures, revealing stripe-like and herringbone-like domain patterns of monoclinic KNN thin films akin to

296 experimental observations. It is further predicted that the herringbone-like domains of
297 $K_{0.9}Na_{0.1}NbO_3$ thin films can transform into stripe-like domains of the orthorhombic a_1/a_2-phase,
298 which is verified by experiments [57,67] (Figure 2c – f). Notably, the three-dimensional model of the
299 domains is essential for acquiring the correct picture of the equilibrium domain arrangement of
300 KNN thin films. For conventional domain structures of (001)-oriented tetragonal or rhombohedral
301 thin films, the domain wall planes are parallel to the low-index planes, e.g., $(110)_{pc}$ or $(101)_{pc}$. In
302 contrast, the domain wall plane of monoclinic KNN thin films is inclined with respect to both the
303 in-plane and out-of-plane directions of the film.

304 To gain insights into the unconventional domain walls of the monoclinic KNN films, Wang
305 *et al.* performed phase-field simulations using preset regular polydomains of the M_C- and a_1a_2/M_C-
306 phases to obtain the domain wall planes at equilibrium [98] (Figure 4a,b). It is found that the domain
307 walls in both cases are tilted with respect to the horizontal and vertical directions of the film, as
308 shown in Figure 4a,b. The tilt angles depend on the value of the electrostrictive coefficients,
309 especially the shear component Q_{44}. Measuring Q_{44} of KNN from bulk crystals is challenging; thus,
310 different values were assumed in the literature[33,34,37]. A theoretical approach combining the strain
311 phase equilibrium theory and microelasticity analysis was used to extract plausible Q_{44} and
312 reproduce the domain wall tilt angles as a function of compositions, consistent with experiments
313 [98] (Figure 4c,d). These findings suggest that the phase-field simulation is useful for predicting the
314 domain structures and accurately identifying the domain wall orientations for low-symmetry
315 ferroelectrics[65].

316 Superdomain structures featured by hierarchical assemblies of domain variants with
317 periodicities at different length scales[100] have been identified in KNN thin films. These structures,
318 observed in the M_C- and a_1a_2/M_C-phases, pose challenges in understanding their structural

relationship to their composing domain variants and the local features at the junctions, i.e., the superdomain wall. To answer these questions, Zhou *et al.*[38] performed systematic phase-field simulations to identify the low-energy superdomain structures. The two most stable superdomain structures of the M_C- and a_1a_2/M_C-phases are shown in Figure 5. It is found that the superdomain walls of the M_C-phase contain disrupted polarization vectors in the cross-section, resulting in a three-time larger superdomain wall width than that of the a_1a_2/M_C-phase. The different local polarization structures of the superdomain walls may also explain why the superdomain walls of the a_1a_2/M_C-phase are straight and regular [55] while those of the M_C-phase are zigzag and disordered [51,52]. Additionally, the superdomain structures may exhibit unique functional properties. As suggested by phase-field simulations[39], the superdomain walls show enhanced local piezoelectric responses. For example, by controlling the periodicity of superdomains, the effective piezoelectric coefficient of a_1a_2/M_C-phase KNN films can be improved by 20% and the dielectric permittivity by 40%, as shown in Figure 6.

In addition, we point out a few unaddressed questions regarding the domain structures of ferroelectric KNN thin films. First, the formation conditions of some domain morphology observed in experiments have not yet been well understood, such as the checkerboard-like domains in 52 nm $K_{0.9}Na_{0.1}NbO_3$ thin films on NSO [64] and the stripe-like domains consisting of 180° domain walls in M_A-phase $K_{0.75}Na_{0.25}NbO_3$ on TSO [101,102]. Second, the formation mechanism of the a_1a_2/M_C superdomains in anisotropically strained KNN thin films is not fully clear. In experiments, only one set of ferroelastic domain variants of the M_C-phase, e.g., a_2c, appear in the superdomains, resulting in biased in-plane polarization along the $[1\bar{1}0]_O$ of the scandate substrate. In the phase-field simulations[98], however, it requires anisotropic misfit strains as large as $|\varepsilon_{xx} - \varepsilon_{yy}| \approx 1.0\%$ to stabilize such domain structures, compared to the experimental misfit strain offered by

NSO at around 0.3% [30]. In other words, the anisotropic misfit strain alone cannot explain the preference of the a_2c-phase over the a_1c-phase in forming a_1a_2/M_C superdomains. It is suspected there is self-poling of the in-plane polarization during the film growth associated with the intrinsic structural anisotropy of the $(110)_O$ surface of the scandate substrate, which has also been reported in BFO epitaxial thin films on similar substrates[103]. Further insights need to be gained to address this discrepancy. Third, most of the KNN films reported in experiments so far are grown on substrates without a bottom electrode, while existing phase-field simulations of KNN thin films assume short-circuit boundary conditions at the film surface and the interface between the film and substrates[37–39,98]. It is important to perform a systematic study to comprehensively evaluate the influence of electrical boundary conditions on the formation of domain and superdomain structures.

5 Perspectives and Summary

5.1 Ferroelectric NNO thin films

While experimental studies on ferroelectric phases and domains in NNO thin films have been conducted, phase-field simulations have primarily focused on the K-rich side of KNN[37–39,98]. This disparity arises from lacking a comprehensive thermodynamic model that describes the antiferrodistortive, ferroelectric, and antiferroelectric ordering coupled with stress and electric fields. Recent efforts in modeling other antiferroelectric perovskite oxides[104], such as $PbZrO_3$ (PZO)[69] and Sm-doped BFO[105], provide a potential roadmap for adapting similar models to NNO. Notably, relaxor-like behaviors observed in NNO [106] and KNN thin films [107,108] are intriguing yet remain poorly understood, suggesting a need for unified thermodynamic models encompassing the local structural disorders [109–111].

5.2 Topological polar structures

Emerging research on topological polar structures, such as polar vortices and skyrmions, has captivated the ferroelectric community since their discovery in the heterostructures of perovskite oxides[112,113]. Exploring whether similar and novel topological polar structures can manifest in KNN-based thin films and heterostructures is an enticing prospect, as implied in the recent discovery of polar topological bubbles in KNN-based ceramics[114]. The delicate interplay between bulk, mechanical, and electrical energies may facilitate the formation of these structures in KNN-based superlattices with paraelectric materials such as STO and $KTaO_3$. Moreover, ferroelectric-antiferroelectric superlattices[104] have enabled unprecedented electromechanical responses. As KNN solid solutions can host ferroelectric and antiferroelectric phases by compositional tuning, it is interesting to investigate the feasibility of KNN-based ferroelectric-antiferroelectric superlattices[104]. Along this direction, the theoretical prediction of the multi-dimensional phase diagrams of these heterostructures using phase-field simulations[115,116] would be beneficial for guiding the experimental exploration.

5.3 Domain switching and domain wall dynamics

Despite recent advances in understanding the equilibrium domain structures of KNN thin films, studies on the dynamical behavior of domains and domain walls remain relatively limited, both theoretically[117] and experimentally[25,118]. Recent work has shown the reversible in-plane and out-of-plane polarization switching in M_C-phase KNN thin films with $SrRuO_3$ bottom electrodes using electric bias via a scanning probe[118]. Future investigations should focus on systematic studies of their domain switching dynamics using phase-field simulations and experimental validations. Additionally, exploring mechanical switching of domains, as demonstrated in other ferroelectric

materials like BTO[119], $PbZr_{0.2}Ti_{0.8}O_3$ [120], and BFO thin films[121], presents an intriguing avenue for investigating bidirectional and multistate switching possibilities in KNN thin films.

6 Summary

We reviewed recent advances in understanding the ferroelectric phase equilibria, phase transitions, and equilibrium domain structures of KNN epitaxial thin films, underscoring the pivotal role of phase-field simulations in gaining deep insights. The simulations have facilitated accurate prediction of strain phase diagrams, reconstruction of complex three-dimensional domain configurations, identification of domain wall orientations, and evaluation of the domain size effects on the piezoelectric coefficients, which have significantly advanced our understanding of ferroelectric KNN thin films. Challenges and opportunities lie ahead in refining thermodynamic models for NNO and Na-rich KNN to explore the antiferroelectric phases and domains, employing phase-field approaches to explore the topological polar textures in KNN-based heterostructures, and theoretically elucidating the dynamic behavior of KNN thin films.

To overcome these challenges, we believe that integration between atomistic and mesoscale methods, innovation in phase-field methodology, and proper use of machine learning techniques are of key importance. For example, the parameterization of a phase-field model of ferroelectric materials is often based on empirical fitting of materials properties measured in experiments, which limits its timely applicability to new ferroelectric materials or solid-solutions of known materials[122,123]. The machine-learning interatomic potential allows for exploring structural dynamics and functional properties at finite temperatures with quantum accuracy and can be utilized to determine phase-field parameters of ferroelectric materials from *ab initio*[124,125]. The recently developed multiphase-field model for ferroelectrics offers another avenue for

studying ferroelectric behavior without resorting to the LGD model[126]. Machine learning surrogate models can be used to accelerate the construction of strain phase diagrams and prediction of ferroelectric behaviors under various operation[127,128]. We anticipate the successful implementation of these emerging techniques to study KNN-based ferroelectrics in the near future. In addition, joint efforts between theoretical modeling and experimental investigations are indispensable to uncover new physics and unlock new functionalities of KNN-based crystals[129] and thin films[130], paving the way for their advanced applications in diverse technological domains.

Acknowledgments

Part of this work was performed under the auspices of the U.S. Department of Energy by Lawrence Livermore National Laboratory under Contract DE-AC52-07NA27344. L.-Q. C. acknowledges support from the National Science Foundation (NSF) through Grant No. DMR-2133373. M.-J. Z. acknowledges support from the NSF of China (Grant No.52102141).

Data Availability Statement

Data sharing is not applicable to this article as no new data were created or analyzed in this study.

Conflict of Interest Statement

On behalf of all authors, the corresponding author states that there is no conflict of interest.

Authors Contributions

B. W. had the idea for the article. B. W. performed the literature search and drafted the manuscript. B. W. and M. Z. prepared for the figures. M. Z., T. Y., and L.-Q. C. critically revised the work. All authors read and approved the final manuscript

Funding

This work was funded by the U.S. Department of Energy by Lawrence Livermore National Laboratory under Contract DE-AC52-07NA27344; the National Science Foundation (NSF) through Grant No. DMR- 2133373; and NSF of China (Grant No.52102141).

References

1. N. Setter, D. Damjanovic, L. Eng, G. Fox, S. Gevorgian, S. Hong, A. Kingon, H. Kohlstedt, N. Y. Park, G. B. Stephenson, I. Stolitchnov, A. K. Taganstev, D. V. Taylor, T. Yamada, and S. Streiffer: Ferroelectric thin films: Review of materials, properties, and applications. *Journal of Applied Physics* **100**(5), 051606 (2006).
2. D. Damjanovic: Ferroelectric, dielectric and piezoelectric properties of ferroelectric thin films and ceramics. *Rep. Prog. Phys.* **61**(9), 1267 (1998).
3. J. Ryu, M. Peddigari, B. Wang, R. Wang, W.-H. Yoon, J. Jang, H. Lee, K. Song, G.-T. Hwang, and K. Wang: Artificially tailored relaxor ferroelectrics for high energy density capacitors. (2022).
4. U. K. Bhaskar, N. Banerjee, A. Abdollahi, Z. Wang, D. G. Schlom, G. Rijnders, and G. Catalan: A flexoelectric microelectromechanical system on silicon. *Nature Nanotech* **11**(3), 263 (2016).
5. B. W. Wessels: Ferroelectric Epitaxial Thin Films for Integrated Optics. *Annu. Rev. Mater. Res.* **37**(1), 659 (2007).
6. J. F. Scott and C. A. P. D. Araujo: Ferroelectric Memories. *Science, New Series* **246**(4936), 1400 (1989).

7. D. G. Schlom, L.-Q. Chen, C. J. Fennie, V. Gopalan, D. A. Muller, X. Pan, R. Ramesh, and R. Uecker: Elastic strain engineering of ferroic oxides. *MRS Bull.* **39**(2), 118 (2014).
8. V. Nagarajan, C. S. Ganpule, B. Nagaraj, S. Aggarwal, S. P. Alpay, A. L. Roytburd, E. D. Williams, and R. Ramesh: Effect of mechanical constraint on the dielectric and piezoelectric behavior of epitaxial Pb(Mg1/3Nb2/3)O3(90%)–PbTiO3(10%) relaxor thin films. *Applied Physics Letters* **75**(26), 4183 (1999).
9. K. J. Choi, M. Biegalski, Y. L. Li, A. Sharan, J. Schubert, R. Uecker, P. Reiche, Y. B. Chen, X. Q. Pan, V. Gopalan, L.-Q. Chen, D. G. Schlom, and C. B. Eom: Enhancement of Ferroelectricity in Strained BaTiO3 Thin Films. *Science* **306**(5698), 1005 (2004).
10. D. Sando, A. Barthélémy, and M. Bibes: $BiFeO_3$ epitaxial thin films and devices: past, present and future. *J. Phys.: Condens. Matter* **26**(47), 473201 (2014).
11. R. J. Zeches, M. D. Rossell, J. X. Zhang, A. J. Hatt, Q. He, C.-H. Yang, A. Kumar, C. H. Wang, A. Melville, C. Adamo, G. Sheng, Y.-H. Chu, J. F. Ihlefeld, R. Erni, C. Ederer, V. Gopalan, L. Q. Chen, D. G. Schlom, N. A. Spaldin, L. W. Martin, and R. Ramesh: A Strain-Driven Morphotropic Phase Boundary in $BiFeO_3$. *Science* **326**(5955), 977 (2009).
12. A. W. Hewat: Cubic-tetragonal-orthorhombic-rhombohedral ferroelectric transitions in perovskite potassium niobate: neutron powder profile refinement of the structures. *J. Phys. C: Solid State Phys.* **6**(16), 2559 (1973).
13. S. L. Skjærvø, K. Høydalsvik, A. B. Blichfeld, M.-A. Einarsrud, and T. Grande: Thermal evolution of the crystal structure and phase transitions of $KNbO_3$. *R. Soc. open sci.* **5**(6), 180368 (2018).
14. N. Ishizawa, J. Wang, T. Sakakura, Y. Inagaki, and K. Kakimoto: Structural evolution of Na0.5K0.5NbO3 at high temperatures. *Journal of Solid State Chemistry* **183**(11), 2731 (2010).
15. B. Orayech, A. Faik, G. A. López, O. Fabelo, and J. M. Igartua: Mode-crystallography analysis of the crystal structures and the low- and high-temperature phase transitions in $Na_{0.5}K_{0.5}NbO_3$. *J Appl Crystallogr* **48**(2), 318 (2015).
16. A. M. Glazer and H. D. Megaw: Studies of the lattice parameters and domains in the phase transitions of NaNbO3. *Acta Cryst A* **29**(5), 489 (1973).
17. R. H. Dungan and R. D. Golding: Metastable Ferroelectric Sodium Niobate. *Journal of the American Ceramic Society* **47**(2), 73 (1964).
18. D. W. Baker, P. A. Thomas, N. Zhang, and A. M. Glazer: A comprehensive study of the phase diagram of KxNa1−xNbO3. *Appl. Phys. Lett.* **95**(9), 091903 (2009).
19. H. Jaffe: Piezoelectric ceramics. *Journal of the American Ceramic Society* **41**(11), 494 (1958).
20. A. N. Morozovska, D. V. Karpinsky, D. O. Alikin, A. Abramov, E. A. Eliseev, M. D. Glinchuk, A. D. Yaremkevich, O. M. Fesenko, T. V. Tsebrienko, A. Pakalniškis, A. Kareiva, M. V. Silibin, V. V. Sidski, S. V. Kalinin, and A. L. Kholkin: A combined theoretical and experimental study of the phase coexistence and morphotropic boundaries in ferroelectric-antiferroelectric-antiferrodistortive multiferroics. *Acta Materialia* **213**, 116939 (2021).
21. J. Rödel and J.-F. Li: Lead-free piezoceramics: Status and perspectives. *MRS Bull.* **43**(8), 576 (2018).

22. J.-F. Li, K. Wang, F.-Y. Zhu, L.-Q. Cheng, and F.-Z. Yao: (K,Na)NbO_3-Based Lead-Free Piezoceramics: Fundamental Aspects, Processing Technologies, and Remaining Challenges. *J. Am. Ceram. Soc.* **96**(12), 3677 (2013).
23. L. Hao, Y. Yang, Y. Huan, H. Cheng, Y.-Y. Zhao, Y. Wang, J. Yan, W. Ren, and J. Ouyang: Achieving a high dielectric tunability in strain-engineered tetragonal K0.5Na0.5NbO3 films. *npj Comput Mater* **7**(1), 62 (2021).
24. H. Liu, H. Wu, K. P. Ong, T. Yang, P. Yang, P. K. Das, X. Chi, Y. Zhang, C. Diao, W. K. A. Wong, E. P. Chew, Y. F. Chen, C. K. I. Tan, A. Rusydi, M. B. H. Breese, D. J. Singh, L.-Q. Chen, S. J. Pennycook, and K. Yao: Giant piezoelectricity in oxide thin films with nanopillar structure. *Science* **369**(6501), 292 (2020).
25. X. Yuan, K. Okamoto, M. Kawano, M. Yoshino, T. Nagasaki, Y. Imai, O. Sakata, and T. Yamada: Extraordinarily Large Contribution Ratio of Ferroelastic Domain Switching to Piezoresponse in Monoclinic (K, Na)NbO3 Films. *Advanced Electronic Materials* **10**(1), 2300405 (2024).
26. S. Liang, D. Finck, M. W. Neis, J. Schwarzkopf, D. Mayer, and R. Wördenweber: SAW gas sensor based on extremely thin strain-engineered K0.7Na0.3NbO3 films. *Applied Physics Letters* **119**(11), 112905 (2021).
27. A. Dejneka and M. Tyunina: Elasto-optic behaviour in epitaxial films of perovskite oxide ferroelectrics. *Advances in Applied Ceramics* **117**(1), 62 (2018).
28. J. Koruza, H. Liu, M. Höfling, M.-H. Zhang, and P. Veber: (K,Na)NbO3-based piezoelectric single crystals: Growth methods, properties, and applications. *Journal of Materials Research* **35**(8), 990 (2020).
29. S.-W. Zhang, Z. Zhou, J. Luo, and J.-F. Li: Potassium-Sodium-Niobate-Based Thin Films: Lead Free for Micro-Piezoelectrics. *Annalen der Physik* **531**(7), 1800525 (2019).
30. J. Schwarzkopf, D. Braun, M. Hanke, R. Uecker, and M. Schmidbauer: Strain Engineering of Ferroelectric Domains in KxNa1−xNbO3 Epitaxial Layers. *Front. Mater.* **4**, 26 (2017).
31. S. R. Burns and M. R. Dolgos: Sizing up (K 1−x Na x)NbO 3 films: a review of synthesis routes, properties & applications. *New Journal of Chemistry* **45**(17), 7408 (2021).
32. H. Pohlmann, J.-J. Wang, B. Wang, and L.-Q. Chen: A thermodynamic potential and the temperature-composition phase diagram for single-crystalline $K_{1-x}Na_xNbO_3$ ($0 \leq x \leq 0.5$). *Appl. Phys. Lett.* **110**(10), 102906 (2017).
33. M.-J. Zhou, J.-J. Wang, L.-Q. Chen, and C.-W. Nan: Strain, temperature, and electric-field effects on the phase transition and piezoelectric responses of $K_{0.5}Na_{0.5}NbO_3$ thin films. *Journal of Applied Physics* **123**(15), 154106 (2018).
34. X. Zhao, J.-J. Wang, and L.-Q. Chen: A thermodynamic study of phase transitions and electrocaloric properties of K0.5Na0.5NbO3 single crystals. *Applied Physics Letters* **116**(9), 092902 (2020).
35. W. Li, C. Chen, G. Xie, and Y. Su: Optimizing K0.5Na0.5NbO3 Single Crystal by Engineering Piezoelectric Anisotropy. *Nanomaterials* **11**(7), 1753 (2021).
36. L.-Q. Chen: Phase-Field Method of Phase Transitions/Domain Structures in Ferroelectric Thin Films: A Review. *J American Ceramic Society* **91**(6), 1835 (2008).

37. B. Wang, H.-N. Chen, J.-J. Wang, and L.-Q. Chen: Ferroelectric domain structures and temperature-misfit strain phase diagrams of $K_{1-x}Na_xNbO_3$ thin films: A phase-field study. *Appl. Phys. Lett.* **115**(9), 092902 (2019).
38. M.-J. Zhou, B. Wang, A. Ladera, L. Bogula, H.-X. Liu, L.-Q. Chen, and C.-W. Nan: Phase diagrams, superdomains, and superdomain walls in K Na1-NbO3 epitaxial thin films. *Acta Materialia* **215**, 117038 (2021).
39. M.-J. Zhou, B. Wang, K. Peng, H.-X. Liu, L.-Q. Chen, and C.-W. Nan: Phase-field simulation of domain size effect on dielectric and piezoelectric responses in K0.5Na0.5NbO3 epitaxial thin films with superdomain structures. *Acta Materialia* **248**, 118777 (2023).
40. I. Fujii, S. Tagata, T. Nakao, N. Koyama, H. Adachi, and T. Wada: Fabrication of $(K,Na)NbO_3$ films on $SrRuO_3$/(001)$SrTiO_3$ substrates by pulsed laser deposition. *Jpn. J. Appl. Phys.* **54**(10S), 10NA13 (2015).
41. S. Pradhan, M. Rath, A. David, D. Kumar, W. Prellier, and M. S. R. Rao: Thickness-Dependent Domain Relaxation Dynamics Study in Epitaxial K0.5Na0.5NbO3 Ferroelectric Thin Films. *ACS Appl. Mater. Interfaces* **13**(30), 36407 (2021).
42. C. Groppi, F. Maspero, M. Asa, G. Pavese, C. Rinaldi, E. Albisetti, M. Badillo-Avila, and R. Bertacco: Spontaneous pattern of orthogonal ferroelectric domains in epitaxial KNN films. *Journal of Applied Physics* **134**(20), 204102 (2023).
43. R. Xu, K. J. Crust, V. Harbola, R. Arras, K. Y. Patel, S. Prosandeev, H. Cao, Y.-T. Shao, P. Behera, L. Caretta, W. J. Kim, A. Khandelwal, M. Acharya, M. M. Wang, Y. Liu, E. S. Barnard, A. Raja, L. W. Martin, X. W. Gu, H. Zhou, R. Ramesh, D. A. Muller, L. Bellaiche, and H. Y. Hwang: Size-Induced Ferroelectricity in Antiferroelectric Oxide Membranes. *Advanced Materials* **35**(17), 2210562 (2023).
44. T. Shiraishi, H. Einishi, S. Yasui, M. Ishikawa, T. Hasegawa, M. Kurosawa, H. Uchida, Y. Sakashita, and H. Funakubo: Growth of Epitaxial 100-Oriented $KNbO_3$–$NaNbO_3$ Solid Solution Films on $(100)_c SrRuO_3$ ‖(100)$SrTiO_3$ by Hydrothermal Method and Their Characterization. *Jpn. J. Appl. Phys.* **50**(9S2), 09ND11 (2011).
45. K. Suenaga, K. Shibata, K. Watanabe, A. Nomoto, F. Horikiri, and T. Mishima: Effect of Lattice Strain and Improvement of the Piezoelectric Properties of (K,Na)NbO3 Lead-Free Film. *Jpn. J. Appl. Phys.* **49**(9S), 09MA05 (2010).
46. G. Tan, S. H. Kweon, K. Shibata, T. Yamada, and I. Kanno: In Situ XRD Observation of Crystal Deformation of Piezoelectric (K,Na)NbO3 Thin Films. *ACS Appl. Electron. Mater.* **2**(7), 2084 (2020).
47. K. Tanaka, Y. Kawata, S. H. Kweon, G. Tan, T. Yoshimura, and I. Kanno: Crystal structure and piezoelectric properties of lead-free epitaxial (K,Na)NbO3 thin films grown on Si substrates. *Applied Physics Letters* **121**(17), 172901 (2022).
48. K.-N. Pham, N. H. Gaukås, M. Morozov, T. Tybell, P. E. Vullum, T. Grande, and M.-A. Einarsrud: Epitaxial $K_{0.5}Na_{0.5}NbO_3$ thin films by aqueous chemical solution deposition. *R. Soc. open sci.* **6**(1), 180989 (2019).
49. J. Luo, W. Sun, Z. Zhou, H.-Y. Lee, K. Wang, F. Zhu, Y. Bai, Z. J. Wang, and J.-F. Li: Monoclinic (K,Na)NbO3 Ferroelectric Phase in Epitaxial Films. *Advanced Electronic Materials* **3**(10), 1700226 (2017).

50. P.-E. Janolin: Strain on ferroelectric thin films: Example of Pb(Zr1−xTix)O3. *J Mater Sci* **44**(19), 5025 (2009).
51. L. von Helden, L. Bogula, P.-E. Janolin, M. Hanke, T. Breuer, M. Schmidbauer, S. Ganschow, and J. Schwarzkopf: Huge impact of compressive strain on phase transition temperatures in epitaxial ferroelectric $K_x Na_{1-x} NbO_3$ thin films. *Appl. Phys. Lett.* **114**(23), 232905 (2019).
52. Y. Wang, S. Bin Anooz, G. Niu, M. Schmidbauer, L. Wang, W. Ren, and J. Schwarzkopf: Thickness effect on ferroelectric domain formation in compressively strained K 0.65 Na 0.35 NbO 3 epitaxial films. *Phys. Rev. Materials* **6**(8), 084413 (2022).
53. L. von Helden, M. Schmidbauer, S. Liang, M. Hanke, R. Wördenweber, and J. Schwarzkopf: Ferroelectric monoclinic phases in strained $K_{0.70} Na_{0.30} NbO_3$ thin films promoting selective surface acoustic wave propagation. *Nanotechnology* **29**(41), 415704 (2018).
54. J. Luo, W. Sun, Z. Zhou, Y. Bai, Z. J. Wang, G. Tian, D. Chen, X. Gao, F. Zhu, and J.-F. Li: Domain Evolution and Piezoelectric Response across Thermotropic Phase Boundary in (K,Na)NbO3-Based Epitaxial Thin Films. *ACS Appl. Mater. Interfaces* **9**(15), 13315 (2017).
55. D. Braun, M. Schmidbauer, M. Hanke, and J. Schwarzkopf: Hierarchy and scaling behavior of multi-rank domain patterns in ferroelectric $K_{0.9} Na_{0.1} NbO_3$ strained films. *Nanotechnology* **29**(1), 015701 (2018).
56. M. Schmidbauer, D. Braun, T. Markurt, M. Hanke, and J. Schwarzkopf: Strain engineering of monoclinic domains in $K_x Na_{1-x} NbO_3$ epitaxial layers: a pathway to enhanced piezoelectric properties. *Nanotechnology* **28**(24), 24LT02 (2017).
57. M. Schmidbauer, L. Bogula, B. Wang, M. Hanke, L. von Helden, A. Ladera, J.-J. Wang, L.-Q. Chen, and J. Schwarzkopf: Temperature dependence of three-dimensional domain wall arrangement in ferroelectric K0. 9Na0. 1NbO3 epitaxial thin films. *Journal of Applied Physics* **128**(18), 184101 (2020).
58. J. Schwarzkopf, D. Braun, M. Schmidbauer, A. Duk, and R. Wördenweber: Ferroelectric domain structure of anisotropically strained $NaNbO_3$ epitaxial thin films. *Journal of Applied Physics* **115**(20), 204105 (2014).
59. J. Schwarzkopf, M. Schmidbauer, T. Remmele, A. Duk, A. Kwasniewski, S. Bin Anooz, A. Devi, and R. Fornari: Strain-induced phase transitions in epitaxial $NaNbO_3$ thin films grown by metal–organic chemical vapour deposition. *J Appl Crystallogr* **45**(5), 1015 (2012).
60. M. Schmidbauer, J. Sellmann, D. Braun, A. Kwasniewski, A. Duk, and J. Schwarzkopf: Ferroelectric domain structure of NaNbO3 epitaxial thin films grown on (110) DyScO3 substrates. *physica status solidi (RRL) – Rapid Research Letters* **8**(6), 522 (2014).
61. T. Schneider, J. Cardoletti, P. Komissinskiy, and L. Alff: Impact of Strain Engineering on Antiferroelectricity in NaNbO3 Thin Films. *ACS Omega* **8**(26), 23587 (2023).
62. M. de Oliveira Guimarães, C. Richter, M. Hanke, S. Bin Anooz, Y. Wang, J. Schwarzkopf, and M. Schmidbauer: Ferroelectric phase transitions in tensile-strained $NaNbO_3$ epitaxial films probed by *in situ* x-ray diffraction. *Journal of Applied Physics* **132**(15), 154102 (2022).

63. J. Luo, L. Liu, S.-W. Zhang, and J.-F. Li: Ferroelectric Domain Structures in Monoclinic (K0.5Na0.5)NbO3 Epitaxial Thin Films. *physica status solidi (RRL) – Rapid Research Letters* **15**(6), 2100127 (2021).
64. D. Braun, M. Schmidbauer, M. Hanke, A. Kwasniewski, and J. Schwarzkopf: Tunable ferroelectric domain wall alignment in strained monoclinic $K_x Na_{1-x} NbO_3$ epitaxial films. *Appl. Phys. Lett.* **110**(23), 232903 (2017).
65. I. Biran and S. Gorfman: Permissible domain walls in monoclinic MAB ferroelectric phases. *Acta Cryst A* **80**(1) (2024).
66. J. Fousek: Permissible domain walls in ferroelectric species. *Czech J Phys* **21**(9), 955 (1971).
67. L. Bogula, L. Von Helden, C. Richter, M. Hanke, J. Schwarzkopf, and M. Schmidbauer: Ferroelectric phase transitions in multi-domain $K_{0.9} Na_{0.1} NbO_3$ epitaxial thin films. *Nano Futures* **4**(3), 035005 (2020).
68. N. A. Pertsev, A. K. Tagantsev, and N. Setter: Phase transitions and strain-induced ferroelectricity in SrTiO 3 epitaxial thin films. *Phys. Rev. B* **61**(2), R825 (2000).
69. Z. Liu and B.-X. Xu: Insight into perovskite antiferroelectric phases: Landau theory and phase field study. *Scripta Materialia* **186**, 136 (2020).
70. D. M. Hatch and H. T. Stokes: Complete listing of order parameters for a crystalline phase transition: A solution to the generalized inverse Landau problem. *Phys. Rev. B* **65**(1), 014113 (2001).
71. B. Wang, Y. Gu, S. Zhang, and L.-Q. Chen: Flexoelectricity in solids: Progress, challenges, and perspectives. *Progress in Materials Science* **106**, 100570 (2019).
72. L. Guin and D. M. Kochmann: A phase-field model for ferroelectrics with general kinetics, Part I: Model formulation. *Journal of the Mechanics and Physics of Solids* **176**, 105301 (2023).
73. T. Yang, B. Wang, J.-M. Hu, and L.-Q. Chen: Domain Dynamics under Ultrafast Electric-Field Pulses. *Phys. Rev. Lett.* **124**(10), 107601 (2020).
74. H. Akamatsu, Y. Yuan, V. A. Stoica, G. Stone, T. Yang, Z. Hong, S. Lei, Y. Zhu, R. C. Haislmaier, J. W. Freeland, L.-Q. Chen, H. Wen, and V. Gopalan: Light-Activated Gigahertz Ferroelectric Domain Dynamics. *Phys. Rev. Lett.* **120**(9), 096101 (2018).
75. S. Zhuang and J.-M. Hu: Role of polarization-photon coupling in ultrafast terahertz excitation of ferroelectrics. *Phys. Rev. B* **106**(14), L140302 (2022).
76. H.-L. Hu and L.-Q. Chen: Three-Dimensional Computer Simulation of Ferroelectric Domain Formation. *Journal of the American Ceramic Society* **81**(3), 492 (1998).
77. Y. L. Li, S. Y. Hu, Z. K. Liu, and L. Q. Chen: Effect of substrate constraint on the stability and evolution of ferroelectric domain structures in thin films. *Acta Materialia* **50**(2), 395 (2002).
78. Y. L. Li, S. Y. Hu, Z. K. Liu, and L. Q. Chen: Effect of electrical boundary conditions on ferroelectric domain structures in thin films. *Appl. Phys. Lett.* **81**(3), 427 (2002).
79. J.-J. Wang, B. Wang, and L.-Q. Chen: Understanding, Predicting, and Designing Ferroelectric Domain Structures and Switching Guided by the Phase-Field Method. *Annu. Rev. Mater. Res.* **49**(1), 127 (2019).

80. D. Schrade, R. Mueller, B. X. Xu, and D. Gross: Domain evolution in ferroelectric materials: A continuum phase field model and finite element implementation. *Computer Methods in Applied Mechanics and Engineering* **196**(41–44), 4365 (2007).
81. L. Liang, Y. L. Li, L.-Q. Chen, S. Y. Hu, and G.-H. Lu: A thermodynamic free energy function for potassium niobate. *Appl. Phys. Lett.* **94**(7), 072904 (2009).
82. L. Liang, Y. L. Li, L.-Q. Chen, S. Y. Hu, and G.-H. Lu: Thermodynamics and ferroelectric properties of KNbO3. *Journal of Applied Physics* **106**(10), 104118 (2009).
83. N. A. Pertsev, A. G. Zembilgotov, and A. K. Tagantsev: Effect of Mechanical Boundary Conditions on Phase Diagrams of Epitaxial Ferroelectric Thin Films. *Phys. Rev. Lett.* **80**(9), 1988 (1998).
84. D. Liu, G. Bai, and C. Gao: Phase diagrams classification based on machine learning and phenomenological investigation of physical properties in K1 − xNaxNbO3 thin films. *Journal of Applied Physics* **127**(15), 154101 (2020).
85. Y. Wu, Y. Ou, J. Peng, and C. Lei: Phase Structures, Electromechanical Responses, and Electrocaloric Effects in K0.5Na0.5NbO3 Epitaxial Film Controlled by Non-Isometric Misfit Strain. *Crystals* **13**(9), 1321 (2023).
86. N. Hadaeghi, M. Dai, Y. Zhang, R. Xie, H. Nouri, and H. Zhang: Origin of antiferroelectricity in NaNbO3. *Phys. Rev. Mater.* **8**(1), 015004 (2024).
87. K. Patel, S. Prosandeev, B. Xu, C. Xu, and L. Bellaiche: Properties of (001) NaNbO 3 films under epitaxial strain: A first-principles study. *Phys. Rev. B* **103**(9), 094103 (2021).
88. K. Kim, W. Hwang, J.-H. Lee, and A. Soon: Explicating the irreversible electric-field-assisted ferroelectric phase transition in the otherwise antiferroelectric sodium niobate for energy storage systems. *J. Mater. Chem. C* **10**(29), 10500 (2022).
89. O. Diéguez, K. M. Rabe, and D. Vanderbilt: First-principles study of epitaxial strain in perovskites. *Phys. Rev. B* **72**(14), 144101 (2005).
90. G. Bai and W. Ma: Phenomenological analysis of phase transitions in epitaxial perovskite ferroelectric thin films. *Physica B: Condensed Matter* **405**(7), 1901 (2010).
91. Q. Li, L. Liu, Y. Ye, J. B. Lv, H. F. Cao, and X. X. Sheng: Phase Structures and Electromechanical Properties of Differently Oriented Epitaxial $K_{0.5}Na_{0.5}NbO_3$ Thin Films. *Acta Phys. Pol. A* **145**(4), 175 (2024).
92. B.-K. Lai, I. A. Kornev, L. Bellaiche, and G. J. Salamo: Phase diagrams of epitaxial BaTiO3 ultrathin films from first principles. *Applied Physics Letters* **86**(13), 132904 (2005).
93. A. Grünebohm, M. Marathe, and C. Ederer: Ab initio phase diagram of BaTiO3 under epitaxial strain revisited. *Applied Physics Letters* **107**(10), 102901 (2015).
94. N. A. Pertsev and V. G. Koukhar: Polarization Instability in Polydomain Ferroelectric Epitaxial Thin Films and the Formation of Heterophase Structures. *Phys. Rev. Lett.* **84**(16), 3722 (2000).
95. S. P. Alpay and A. L. Roytburd: Thermodynamics of polydomain heterostructures. III. Domain stability map. *Journal of Applied Physics* **83**(9), 4714 (1998).
96. F. Xue, Y. Ji, and L.-Q. Chen: Theory of strain phase separation and strain spinodal: Applications to ferroelastic and ferroelectric systems. *Acta Materialia* **133**, 147 (2017).
97. B. Wang and L.-Q. Chen: Theory of strain phase equilibria and diagrams. *Acta Materialia* **274**, 120025 (2024).

98. B. Wang: Strain phase equilibria and phase-field method of ferroelectric polydomain: A case study of monoclinic KxNa1- xNbO3 films. *Journal of the American Ceramic Society* **in press** (2024).
99. J. Zorn: Ferroelectric Materials by Design at the Mesoscale: Thermodynamic and Phase-Field Modeling, The Pennsylvania State University, 2022.
100. P. S. Bednyakov and J. Hlinka: Charged Domain Walls in BaTiO3 Crystals Emerging from Superdomain Boundaries. *Advanced Electronic Materials* **9**(6), 2300005 (2023).
101. M. Schmidbauer, M. Hanke, A. Kwasniewski, D. Braun, L. Von Helden, C. Feldt, S. J. Leake, and J. Schwarzkopf: Scanning X-ray nanodiffraction from ferroelectric domains in strained $K_{0.75}Na_{0.25}NbO_3$ epitaxial films grown on (110) $TbScO_3$. *J Appl Crystallogr* **50**(2), 519 (2017).
102. J. Schwarzkopf, D. Braun, M. Hanke, A. Kwasniewski, J. Sellmann, and M. Schmidbauer: Monoclinic MA domains in anisotropically strained ferroelectric K0.75Na0.25NbO3 films on (110) TbScO3 grown by MOCVD. *J Appl Cryst* **49**(2), 375 (2016).
103. C. Beekman, W. Siemons, M. Chi, N. Balke, J. Y. Howe, T. Z. Ward, P. Maksymovych, J. D. Budai, J. Z. Tischler, R. Xu, W. Liu, and H. M. Christen: Ferroelectric Self-Poling, Switching, and Monoclinic Domain Configuration in BiFeO3 Thin Films. *Advanced Functional Materials* **26**(28), 5166 (2016).
104. Y. Si, T. Zhang, C. Liu, S. Das, B. Xu, R. G. Burkovsky, X.-K. Wei, and Z. Chen: Antiferroelectric oxide thin-films: Fundamentals, properties, and applications. *Progress in Materials Science* **142**, 101231 (2024).
105. F. Xue, L. Liang, Y. Gu, I. Takeuchi, S. V. Kalinin, and L.-Q. Chen: Composition- and pressure-induced ferroelectric to antiferroelectric phase transitions in Sm-doped $BiFeO_3$ system. *Appl. Phys. Lett.* **106**(1), 012903 (2015).
106. B. Cai, J. Schwarzkopf, E. Hollmann, D. Braun, M. Schmidbauer, T. Grellmann, and R. Wördenweber: Electronic characterization of polar nanoregions in relaxor-type ferroelectric NaNbO3 films. *Phys. Rev. B* **93**(22), 224107 (2016).
107. S. Liang, Y. Dai, L. von Helden, J. Schwarzkopf, and R. Wördenweber: Surface acoustic waves in strain-engineered K0.7Na0.3NbO3 thin films. *Applied Physics Letters* **113**(5), 052901 (2018).
108. S. Liang, D. Pfützenreuter, D. Finck, L. von Helden, J. Schwarzkopf, and R. Wördenweber: Tunable surface acoustic waves on strain-engineered relaxor K0.7Na0.3NbO3 thin films. *Applied Physics Letters* **116**(5), 052902 (2020).
109. I. Levin, V. Krayzman, G. Cibin, M. G. Tucker, M. Eremenko, K. Chapman, and R. L. Paul: Coupling of emergent octahedral rotations to polarization in (K,Na)NbO3 ferroelectrics. *Sci Rep* **7**(1), 15620 (2017).
110. J. Kong, J. Liu, F. Marlton, M. R. V. Jørgensen, and A. Pramanick: Local structural mechanism for phase transition and ferroelectric polarization in the mixed oxide K0.5Na0.5NbO3. *Phys. Rev. B* **103**(18), 184104 (2021).
111. Z. Tan, Y. Peng, J. An, Q. Zhang, and J. Zhu: Critical Role of Order–Disorder Behavior in Perovskite Ferroelectric KNbO3. *Inorg. Chem.* **60**(11), 7961 (2021).

112. S. Das, Y. Tang, Z. Hong, M. Gonçalves, M. McCarter, C. Klewe, K. Nguyen, F. Gómez-Ortiz, P. Shafer, and E. Arenholz: Observation of room-temperature polar skyrmions. *Nature* **568**(7752), 368 (2019).
113. A. K. Yadav, C. T. Nelson, S. L. Hsu, Z. Hong, J. D. Clarkson, C. M. Schlepütz, A. R. Damodaran, P. Shafer, E. Arenholz, L. R. Dedon, D. Chen, A. Vishwanath, A. M. Minor, L. Q. Chen, J. F. Scott, L. W. Martin, and R. Ramesh: Observation of polar vortices in oxide superlattices. *Nature* **530**(7589), 198 (2016).
114. G. Tian, C. Yang, W. Kuai, Z. Gai, W. Su, J. Du, T. Liu, Y. Zhang, M. Zhao, X. Wang, and L. Zheng: Polar topological bubbles in (K,Na)NbO3-based single crystals via synergetic phase and defect engineering. *Ceramics International* **50**(17, Part A), 29642 (2024).
115. Z. Hong, A. R. Damodaran, F. Xue, S.-L. Hsu, J. Britson, A. K. Yadav, C. T. Nelson, J.-J. Wang, J. F. Scott, L. W. Martin, R. Ramesh, and L.-Q. Chen: Stability of Polar Vortex Lattice in Ferroelectric Superlattices. *Nano Lett.* **17**(4), 2246 (2017).
116. J. Liu, Y. Liu, S. Lan, B. Yang, L. Dou, L. Yang, X. Kong, C.-W. Nan, and Y.-H. Lin: Static structures and dynamic responses of polar topologies in oxide superlattices. *Applied Physics Letters* **121**(21), 212902 (2022).
117. J. Cao, M. Liu, Z. Liu, H. Hou, and Y. Zhao: Alternating Current Field Effects in Atomically Ferroelectric Ultrathin Films. *Materials* **15**(7), 2506 (2022).
118. Y. Wang, S. B. Anooz, G. Niu, J. Zhao, M. Schmidbauer, L. Wang, W. Ren, and J. Schwarzkopf: Evolution of domain structure in epitaxial ferroelectric K 0.5 N a 0.5 Nb O 3 films grown by metal-organic vapor-phase epitaxy. *Phys. Rev. Materials* **8**(5), 054409 (2024).
119. H. Lu, C.-W. Bark, D. Esque de los Ojos, J. Alcala, C. B. Eom, G. Catalan, and A. Gruverman: Mechanical Writing of Ferroelectric Polarization. *Science* **336**(6077), 59 (2012).
120. Q. Li, B. Wang, Q. He, P. Yu, L.-Q. Chen, S. V. Kalinin, and J.-F. Li: Ferroelastic Nanodomain-mediated Mechanical Switching of Ferroelectricity in Thick Epitaxial Films. *Nano Lett.* **21**(1), 445 (2021).
121. S. M. Park, B. Wang, S. Das, S. C. Chae, J.-S. Chung, J.-G. Yoon, L.-Q. Chen, S. M. Yang, and T. W. Noh: Selective control of multiple ferroelectric switching pathways using a trailing flexoelectric field. *Nature Nanotech* **13**(5), 366 (2018).
122. A. M. Ross and L.-Q. Chen: Thermodynamics and Ferroelectric Properties of Pb1-xSrxTiO3 Solid Solutions. *Acta Materialia* **261**, 119405 (2023).
123. M. Liu, C. Hu, X. Meng, X. Sun, Y. Zhang, B. Xing, M. Qiu, Y. Dong, S. Jin, and H. Tian: Thermodynamic potential construction and biaxial stress analysis of K0.4Na0.6NbO3 single crystals. *Applied Physics Letters* **125**(11), 112901 (2024).
124. Y. Hu, J. Yang, and S. Liu: Giant Piezoelectric Effects of Topological Structures in Stretched Ferroelectric Membranes. *Phys. Rev. Lett.* **133**(4), 046802 (2024).
125. P. Xie, Y. Chen, W. E, and R. Car: (2022).
126. L. Fan, M. Reder, D. Schneider, M. Hinterstein, and B. Nestler: A phase-field model for ferroelectric materials—Based on the multiphase-field method. *Computational Materials Science* **230**, 112510 (2023).

127. J. A. Zorn and L.-Q. Chen: Machine-learning enabled construction of temperature-strain phase diagrams of ferroelectric thin films. *Journal of Materials Research* **38**(6), 1644 (2023).
128. K. Alhada-Lahbabi, D. Deleruyelle, and B. Gautier: Machine Learning Surrogate Model for Acceleration of Ferroelectric Phase-Field Modeling. *ACS Appl. Electron. Mater.* **5**(7), 3894 (2023).
129. Y. Liu, L. Bian, R. Zhang, J. Fan, D. Huo, B. Shen, H. Huang, X. Shi, D. Wang, and K. Yao: Ultrahigh electromechanical response in (K,Na)NbO3-based lead-free textured piezoceramics. *Applied Physics Reviews* **11**(3), 031415 (2024).
130. B. Lin, K. P. Ong, T. Yang, Q. Zeng, H. K. Hui, Z. Ye, C. Sim, Z. Yen, P. Yang, Y. Dou, X. Li, X. Gao, C. K. I. Tan, Z. S. Lim, S. Zeng, T. Luo, J. Xu, X. Tong, P. W. F. Li, M. Ren, K. Zeng, C. Sun, S. Ramakrishna, M. B. H. Breese, C. Boothroyd, C. Lee, D. J. Singh, Y. M. Lam, and H. Liu: Ultrahigh electromechanical response from competing ferroic orders. *Nature* 1 (2024).

Figure 1

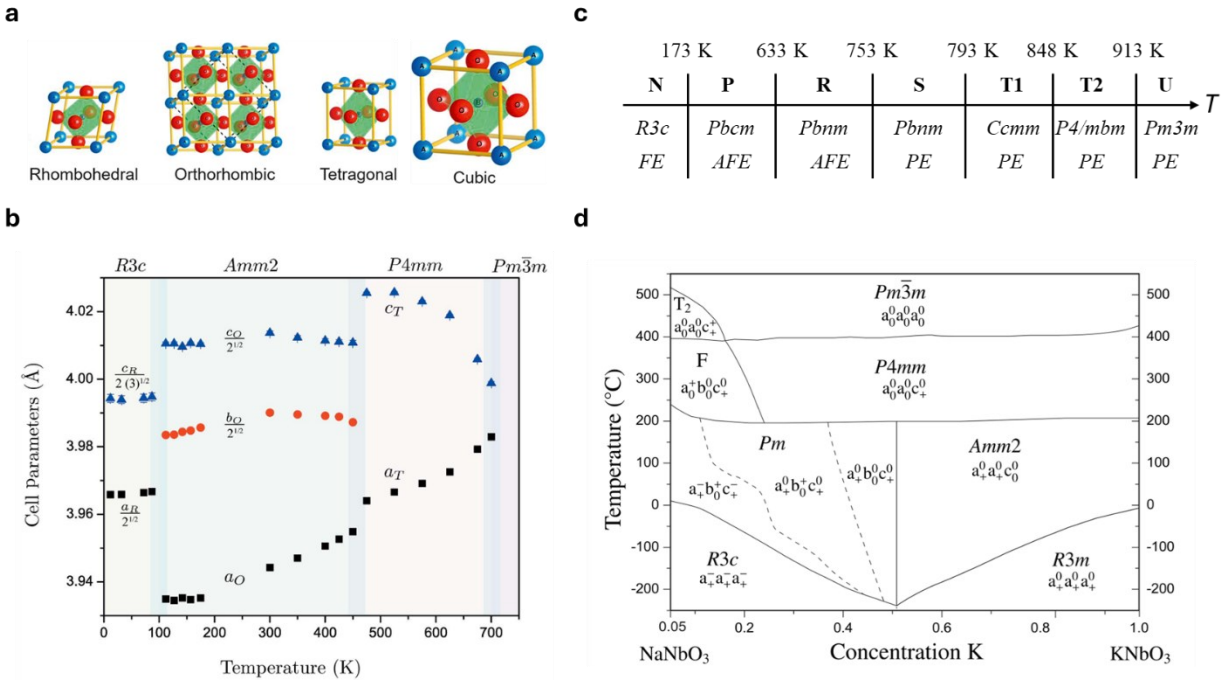

Figure 1. (a) Crystal structures of typical ferroelectric phases of perovskite oxide ABO_3. (b) Phase transition sequence of $K_{0.5}Na_{0.5}NbO_3$ bulk crystals represented by lattice constants and space group. (c) Phase transition sequence of $NaNbO_3$ by space group and polar ordering. PE, FE, and AFE denote paraelectric, ferroelectric, and antiferroelectric, respectively. (d) Phase diagram of $K_xNa_{1-x}NbO_3$ for x = 0.05 to 1.0. The Glazer notations are used to consider both the oxygen octahedral tilt (superscript) and B-site displacements (subscript). (a) is adapted from Ref. 21 with permission. (b) is adapted from Ref. 15 with permission. (c) is adapted from Ref. 86 with permission. (d) is adapted from Ref. 18 with permission.

Figure 2

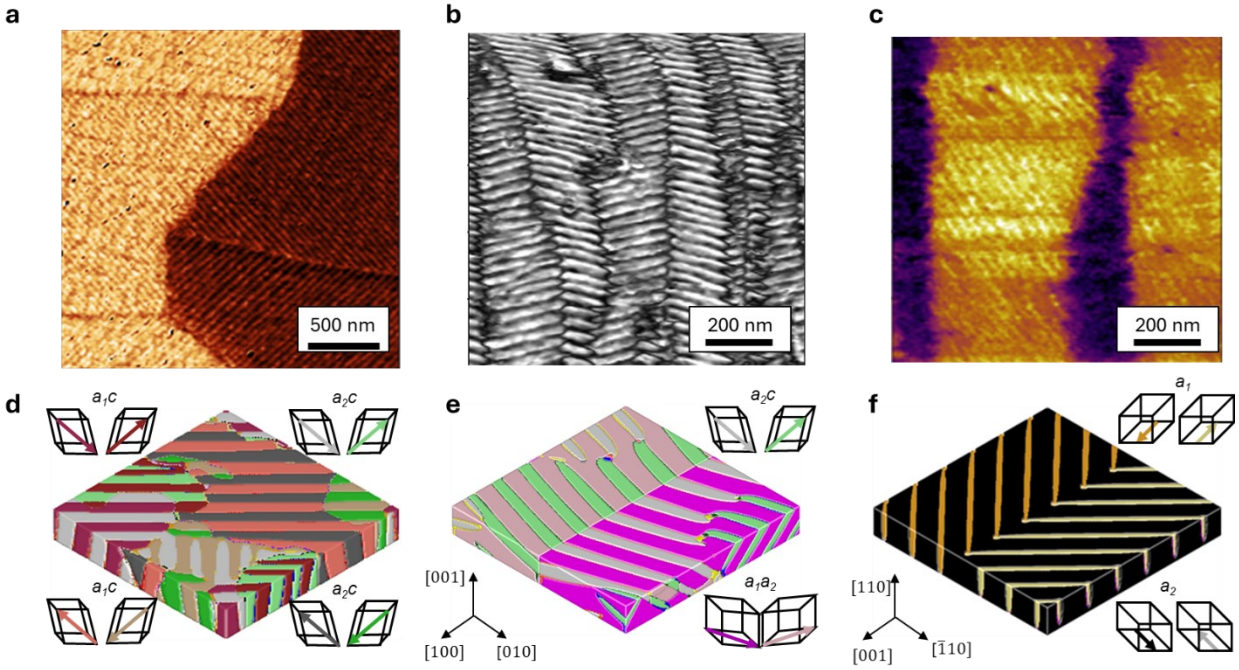

Figure 2. Domain structures of ferroelectric KNN thin films. (a,b,c) Two-dimensional morphology of the ferroelectric domains observed in experiments by piezoresponse force microscopy (PFM) for (a) 35-nm $K_{0.7}Na_{0.3}NbO_3$ film on $TbScO_3$ at room temperature, (b) 30-nm $K_{0.9}Na_{0.1}NbO_3$ film on $NdScO_3$ at room temperature, and (c) 38-nm $K_{0.9}Na_{0.1}NbO_3$ film on $NdScO_3$ at 250 °C. (d,e,f) The corresponding three-dimensional models of the ferroelectric domains obtained from phase-field simulations. (a,b,c) are obtained with the permission of Dr. Martin Schmidbauer and Dr. Jutta Schwarzkopf. (e,f) are adapted from Ref. 57 with permission. (d) is adapted from Ref. 37 with permission.

Figure 3

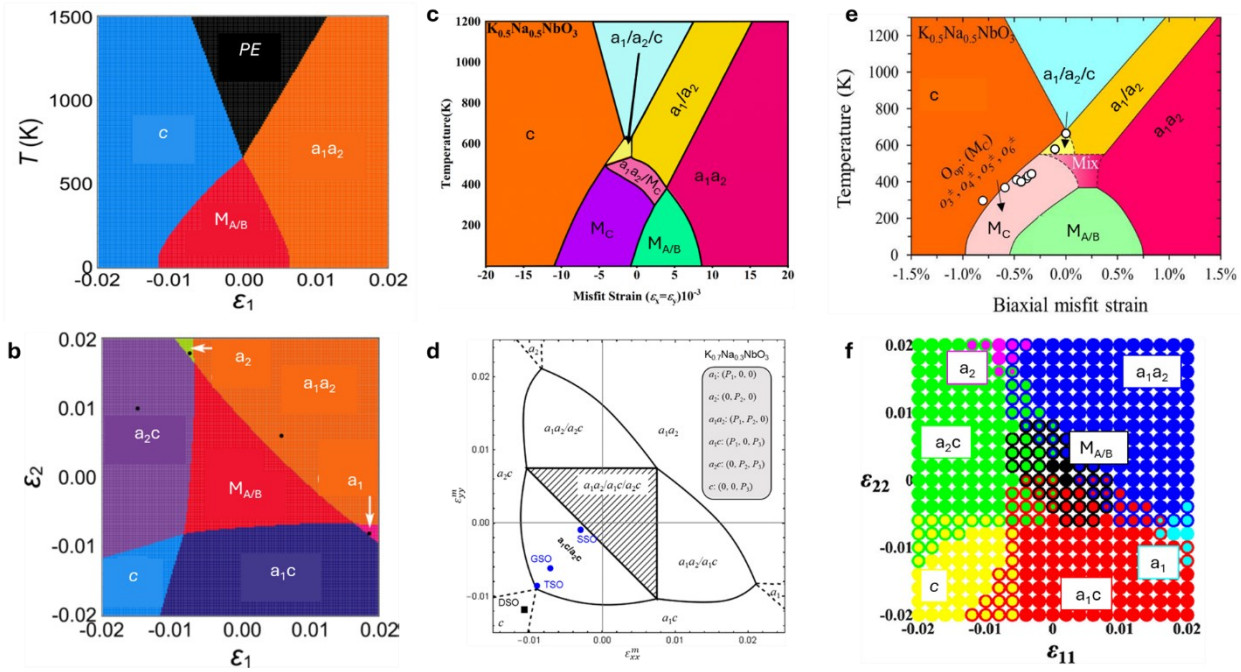

Figure 3. Strain phase diagrams of ferroelectric $K_xNa_{1-x}NbO_3$. (a,c,e) Temperature – strain phase diagrams and (b,d,f) strain – strain phase diagrams at $T = 300$K of $(001)_{pc}$-oriented KNN thin films subjected to biaxial misfit strains. (a,b) are calculated by using the thermodynamic model based on the monodomain assumption. (c,d) are calculated using strain phase equilibrium theory without *a priori* assumptions on the domain structure. (e,f) are calculated using a series of three-dimensional phase-field simulations without *a priori* assumption on the domain structure. (a,b) are adapted from Ref. [33] with permission. (c) is adapted from Ref. [99] with permission. (d) is adapted from Ref. 98 with permission. (e) is adapted from Ref. 37 with permission. (f) is adapted from Ref. 38 with permission.

Figure 4

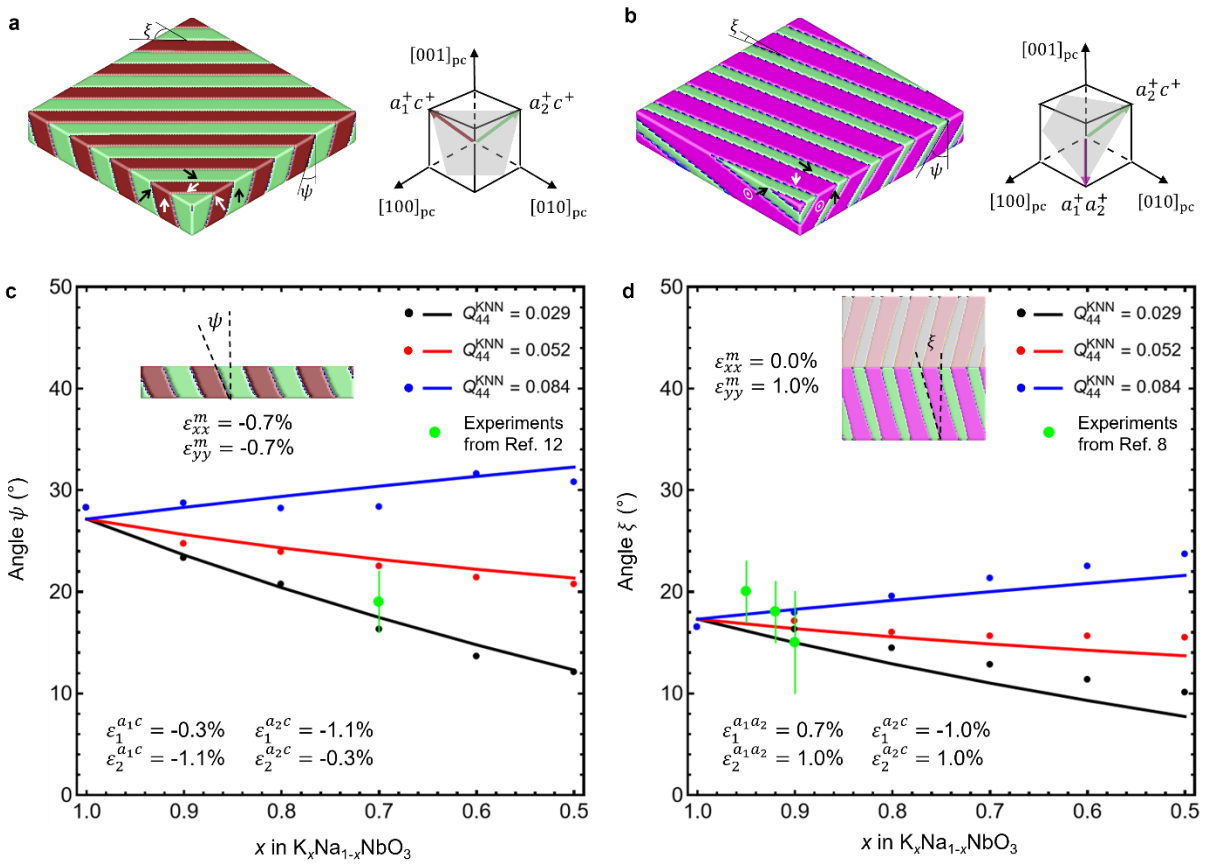

Figure 4. Three-dimensional models of two types of polydomain structures of monoclinic ferroelectric $K_xNa_{1-x}NbO_3$ thin films. (a,b) Domain structures and (c,d) domain wall inclination angles as functions of composition and the electrostrictive coefficients Q_{44} for $K_{0.5}Na_{0.5}NbO_3$ of (a,c) the M_C-phase and (b,d) the a_1a_2/M_C-phase. Adapted from Ref. 98 with permission.

Figure 5

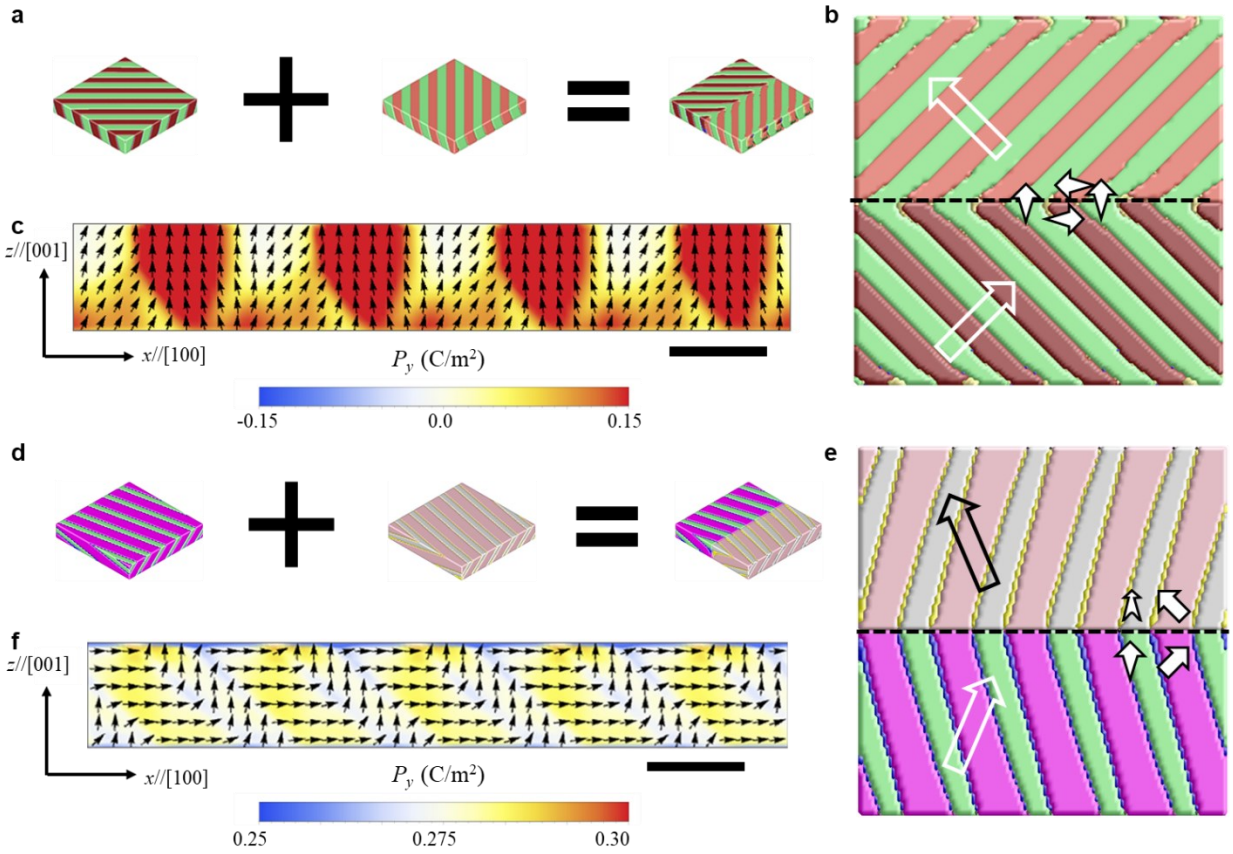

Figure 5. Formation of superdomains by the combination of two bundles of polydomain in monoclinic ferroelectric $K_xNa_{1-x}NbO_3$ thin films. (a,d) Schematics of the merging of two polydomain variants into one period of the superdomain structure case for (a) the M_C-phase and (d) the a_1a_2/M_C-phase. (b,e) planar view of the morphology of near the superdomain boundary indicated by dashed line for (b) the M_C-phase and (e) the a_1a_2/M_C-phase. The direction of the polarization vectors within each domain variant are indicated by solid arrows. The direction of the averaged polarization vectors for each polydomain variant are indicated by large hollow arrows. (c,f) Cross-sectional view of the local polarization vectors within the superdomain boundary for (c) the M_C-phase and (f) the a_1a_2/M_C-phase. The color bar indicates the magnitude of the local polarization vectors. Adapted from Ref. 38 with permission.

Figure 6

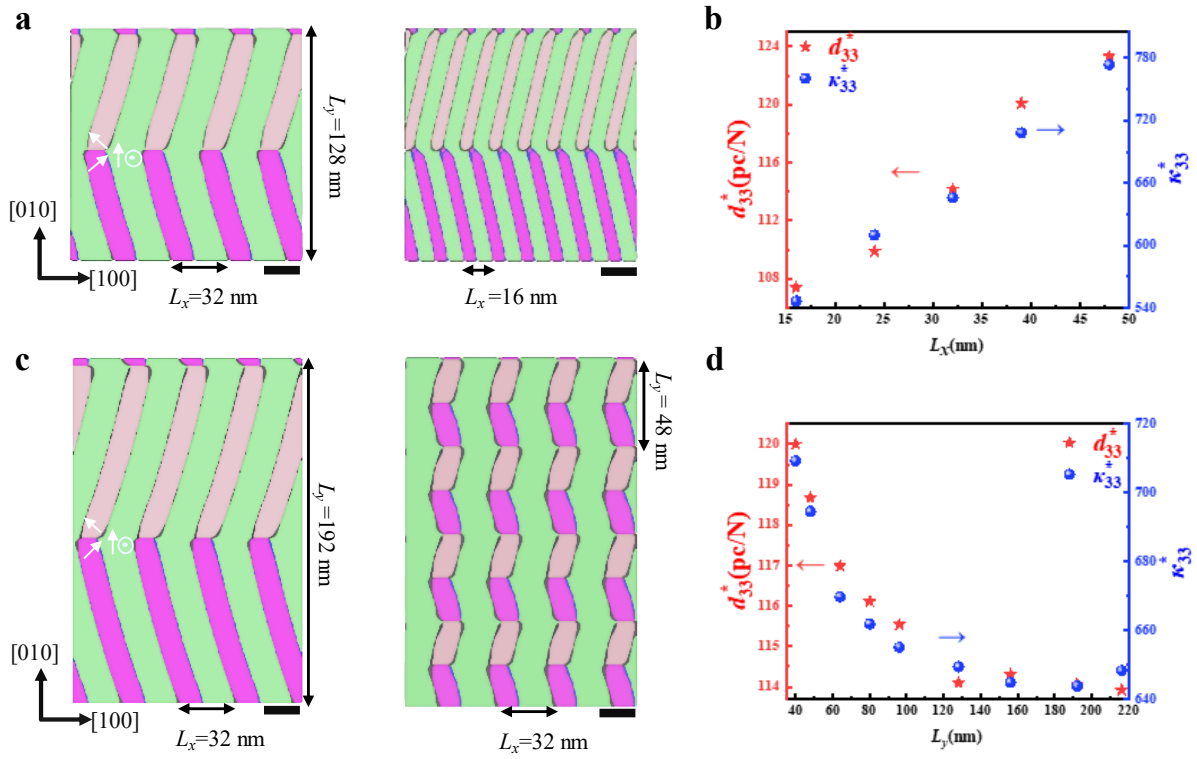

Figure 6. Size effects of domains and superdomains on the overall dielectric and piezoelectric properties of ferroelectric KNN thin films in the a_1a_2/M$_C$-phase. (a,c) Planar view of four domain structures with varied (a) domain periodicity L_x and (c) superdomain periodicity L_y. (b,d) Calculated out-of-plane piezoelectric coefficients d_{33}^* and dielectric permittivity κ_{33}^* of different domain structures as functions of (b) L_x and (d) L_y. Adapted from Ref. 39 with permission.

Table 1. Summary of the ferroelectric phases and domain morphologies of KNN and NNO epitaxial thin films reported in the literature. Abbreviations for substrate materials: $SrTiO_3$(STO), $SmScO_3$ (SSO), $GdScO_3$ (GSO), $NdScO_3$ (NSO), and $TbScO_3$ (TSO).

Phases	*x* of $K_xNa_{1-x}NbO_3$	Substrates	Misfit strains	Temperature (°C)	Domain morphology	Thickness (nm)	Ref.
K-rich side							
Monoclinic (a_1a_2/M_C)	0.90 ~ 0.98	NSO	Biaxially anisotropic	RT	Herringbone	20 ~ 30	56,55,64
Orthorhombic (a_1/a_2)				250	Stripe//[110]pc		57,67
Monoclinic M_A	0.75	TSO		RT	Stripe//[110]pc	29	[101,102]
	0.5, doped	STO		200	-	200	49
Monoclinic M_C	0.54 – 0.74	SSO, GSO, TSO	Biaxially compressive	RT	Stripe//[110]pc	30±10	51,53
	0.5	DSO		RT		32	[118]
	0.5, doped	STO		RT		200	49,54
Orthorhombic (c)	0.7	DSO		RT	Monodomain	30±10	51
	0.54 – 0.74	TSO, GSO, SSO		100 ~ 400			
$NaNbO_3$							
Orthorhombic (c)	0.0	NGO	Compressive	RT	Monodomain	10	58,59
		STO	Slightly compressive	RT		10	58,59
Monoclinic (M_A or M_B)		NGO, DSO, TSO, GSO	Partially relaxed	RT		30 ~ 140	58,59
Monoclinic (a_1a_2)		DSO, TSO, GSO	Tensile	RT	Stripe//[100]pc	1.5 ~ 27	58–60
Orthorhombic (a_1/a_2)		DSO		350	Stripe//[110]pc	42	62

876

877 **Table 2.** Comparison of phases in strained KNN and NNO epitaxial thin films on various substrates
878 at room temperature (RT) and high temperature (HT). Abbreviations for substrate materials:
879 $SrTiO_3$(STO), $SmScO_3$ (SSO), $GdScO_3$ (GSO), $NdScO_3$ (NSO), and $TbScO_3$ (TSO).

Films	**Highly biaxial compressive**	**Moderate biaxial compressive**	**Moderate biaxial tensile**	**Biaxial anisotropic**
KNN (x > 0.5)	RT: orthorhombic c HT: paraelectric	RT: monoclinic M_C HT: orthorhombic c or monoclinic M_A	-	RT: Monoclinic a_1a_2/M_C HT: orthorhombic a_1/a_2
Substrates	STO, DSO	TSO, GSO, SSO	-	NSO
NNO	RT: orthorhombic c	RT: monoclinic M_A or M_B	RT: monoclinic a_1a_2 HT: orthorhombic a_1/a_2	-
Substrates	NGO	STO, partially relaxed NGO, DSO, TSO, GSO	DSO, TSO, GSO	-

880

881

882